94　10　19

內容

　　本結案報告分為兩部分：(一)砷化鎵/砷化鋁異質結構之 $\Gamma - \mathbf{X}$ 反交叉能隙理論分析與(二)以 FTIR 驗證受激載子於能階間之分部情形。第二部分之實驗成果已發表於 J. Appl. Phys. **96**, 4970 (2004)，內容附於此結報中。

砷化鎵／砷化鋁異質結構之Γ－X反交叉能隙理論分析

一、 中文摘要

本研究提供一個非傳統的方法來提供負微分電阻的機制藉以實現兆赫波振盪器。由於砷化鎵/砷化鋁量子井結構中Γ-X混成的效應，其次能帶結構在反交叉能隙的附近曲率會有很大的變化。Γ-X反交叉能隙會是決定Γ-X混成很重要的參數。隨著單位長度的量子井數目的增加Γ-X反交叉能隙也會跟著增加。此外，同一結構中能量較高的次能帶也會有較大的Γ-X反交叉能隙。

關鍵詞：Γ-X mixing、anticrossing gap、GaAs/AlAs、heterostructure、quantum well

Abstract

In this research, we propose a novel idea of negative differential resistance to realize the terahertz oscillator. Because of the Γ-X mixing effect in the GaAs/AlAs multi-quantum well, the curvature of the subband will vary a lot when the anticrossing gap is happened. The magnitude of anticrossing gap is an important parameter. It will increase with the number of wells per unit length. In addition, the higher subband will have a lager Γ-X anticrossing gap.

二、 緣由及目的

近年來兆赫波領域相關的技術在各個領域的應用都被廣泛地被探討[1]。在凝態物理中由於兆赫波段包含了許多重要的能階，如光模聲子(optical phonon)、激子（exiton）的束縛能、半導體的摻雜能階、藍道能級(Landau level)等，兆赫波相關的研究更是顯得重要。雖然兆赫波段在凝態物理上具有極重大的意義，然而近年來其近展並非如預期般迅速。原因是至今仍缺乏高效率、高穩定性、且又符合經濟效益的兆赫波光源。

本研究主要的目的就是要設計能夠到達兆赫波頻段的甘恩振盪器（Gunn oscillator）。而甘恩振盪器是建立在材料具有負微分電阻特性前提上。傳統的甘恩振盪器是利用電子從低能量低等效質量的能谷到高能量高等效質量的能谷間的躍遷來達到負微分電阻，其振盪頻率會受到電子－聲子的散射機率所限制。而在本研究中，我們將會利用砷化鎵/砷化鋁量子井結構中Γ-X混成的效應來達到負微分電阻的特性。在這個機制當中並不須要聲子的參與。所以振盪頻率不會受到電子－聲子的散射機率所限制。

三、 研究報告

3-1 理論架構

在 3.1.1 中我們將利用 empirical pseudopotential method 來計算每一層所對應之塊材的複數能帶結構圖(complex band structure)。在 3.1.2 中我們會利用 3.1.1 所得的塊材波函數當基底搭配散射矩陣法（scattering matrix method）計算次能帶結構(subband structure)。3.1.3 則討論穿透係數(transformission coefficient)的計算。

3-1-1.塊材複數能帶結構圖的理論計算

考慮電子在第 j 層的塊材所滿足的單電子薛丁格方程為

$$[-\nabla^2 + V^j(\mathbf{r}) + U_0^j]\varphi^j(\mathbf{r}) = E\varphi^j(\mathbf{r})。$$

其中 U_0^j 為相對於其它層的 band-offset parameter。利用 Bloch 定理，我們可將第 j 層塊材的波函數用平面波展開：

$$\varphi^j(\mathbf{r}) = e^{i\mathbf{k}^j \cdot \mathbf{r}} u^j(\mathbf{r}) = e^{i\mathbf{k}^j \cdot \mathbf{r}} \sum_{\mathbf{G}} C(\mathbf{k}^j, \mathbf{G}) e^{i\mathbf{G} \cdot \mathbf{r}}$$

此時薛丁格方程可寫為：

$$\sum_{\mathbf{G}'} \overline{H}_{\mathbf{G},\mathbf{G}'}^j(\mathbf{k}^j) C(\mathbf{k}^j, \mathbf{G}) = 0$$

$$\overline{H}_{\mathbf{G},\mathbf{G}'}^j(\mathbf{k}^j) = [(\mathbf{k}^j + \mathbf{G})^2 - E]\delta_{\mathbf{G},\mathbf{G}'} + V^j(|\mathbf{G} - \mathbf{G}'|)$$

其中 $V(|\mathbf{G}-\mathbf{G}'|)$ 為 pseudopotential form factor[2]。

值得注意的是若我們給定能量 E 與平行量子井的波向量 $\mathbf{k}_{\parallel}$，我們可以將 $\overline{H}_{\mathbf{G},\mathbf{G}'}^j(\mathbf{k}^j)$ 寫成 k_z 的二次多項式。

$$\overline{H}_{\mathbf{G},\mathbf{G}'}^j(\mathbf{k}^j) = \overline{H}_{\mathbf{G},\mathbf{G}'}^{j(0)}(\mathbf{k}_{\parallel}) + \overline{H}_{\mathbf{G},\mathbf{G}'}^{(1)}(\mathbf{k}_{\parallel}) k_z + \delta_{\mathbf{G},\mathbf{G}'} (k_z^j)^2$$

$$\overline{H}_{\mathbf{G},\mathbf{G}'}^{j(0)}(\mathbf{k}_{\parallel}) = [|\mathbf{k}_{\parallel}|^2 + |\mathbf{G}|^2 + 2\mathbf{k}_{\parallel} \cdot \mathbf{G} - E]\delta_{\mathbf{G},\mathbf{G}'} + V^j(|\mathbf{G} - \mathbf{G}'|)$$

$$\overline{H}_{\mathbf{G},\mathbf{G}'}^{(1)}(\mathbf{k}_{\parallel}) = 2G_z \delta_{\mathbf{G},\mathbf{G}'}$$

若我們令 $\mathbf{C}^{(1)} \equiv k_z^j \mathbf{C}$。其中 $\mathbf{C}$ 為波函數用平面波展開的係數所對應的行向量。我們可以把問題轉成以 k_z^j 為本徵值的本徵值問題[3]。

$$\begin{bmatrix} \mathbf{0} & \mathbf{1} \\ -\overline{H}^{j(0)}(\mathbf{k}_{\parallel}) & -\overline{H}^{(1)}(\mathbf{k}_{\parallel}) \end{bmatrix} \begin{bmatrix} \mathbf{C} \\ \mathbf{C}^{(1)} \end{bmatrix} = k_z^j \begin{bmatrix} \mathbf{C} \\ \mathbf{C}^{(1)} \end{bmatrix}$$

矩陣對角化後我們即可得到塊材的複數能帶結構圖，相對應的波函數可寫為

$$\varphi_{E,\mathbf{k}_{\parallel}}^{j,s}(\mathbf{r}) = e^{i\mathbf{k}_{\parallel} \cdot \mathbf{r}} e^{i k_z^{j,s} z} u_{\mathbf{k}_{\parallel}}^{j,s}(\mathbf{r})$$

為了簡化符號以下我們都忽略下標 E 與 $\mathbf{k}_{\parallel}$。所以 $\varphi_{E,\mathbf{k}_{\parallel}}^{j,s}(\mathbf{r}) \equiv \varphi^{j,s}$。

3-1-2. 砷化鎵/砷化鋁多層量子井結的次能帶結構圖及穿透係數

為了得到整個系統的次能帶結構，我們把系統的波函數用各層塊材的波函數展開並將其分成向前傳遞與向後傳遞兩個部份。

$$\Psi^j(\mathbf{r}) = \sum_{s \in \{S_f\}} a^{j,s} \varphi^{j,s} + \sum_{s \in \{S_b\}} b^{j,s} \varphi^{j,s}$$

其中 $a^{j,s}$ 與 $b^{j,s}$ 分別對應向前傳遞和向後傳遞波的係數。藉由波函數連續及波函數的一階導數連續的邊界條件我們可以得到每一層之間係數關係。

$$\begin{bmatrix} \mathbf{a}^{(n+1)} \\ \mathbf{b}^{(n+1)} \end{bmatrix} = T(n+1) \begin{bmatrix} \mathbf{a}^{(n)} \\ \mathbf{b}^{(n)} \end{bmatrix} \quad \text{for n=1,2,...,N}$$

其中 $\mathbf{a}^{(n)}$ 與 $\mathbf{b}^{(n)}$ 分別代表著在第 n 層中由 $a^{n,s}$ 與 $b^{n,s}$ 所形成的行向量。當每一層係數間的關係決定之後，所有的散射矩陣（scattering matrix）S(m,n)也跟著決定[4]。散射矩陣決定了任兩層間入射波及散射波之間的關係。

$$\begin{bmatrix} \mathbf{a}^{(n)} \\ \mathbf{b}^{(m)} \end{bmatrix} = S(m,n) \begin{bmatrix} \mathbf{a}^{(m)} \\ \mathbf{b}^{(n)} \end{bmatrix} \quad \text{for m} \le \text{n}$$

利用上式我們可推得：

$$\mathbf{a}^{(m)} = S_{11}(1,m)\mathbf{a}^{(1)} + S_{12}(1,m)\mathbf{b}^{(m)}$$

$$\mathbf{b}^{(m)} = S_{21}(m,N)\mathbf{a}^{(m)} + S_{22}(m,N)\mathbf{b}^{(N)}$$

接著我們假設沒有從外界入射至系統的波使得們可以令入射波的係數 $\mathbf{a}^{(1)}$ 與 $\mathbf{b}^{(N)}$ 為零來決定局限於系統的能態。此時由上面二式我們得到[5]：

$$[\mathbf{1} - S_{21}(m,N)S_{12}(1,m)]\mathbf{b}^{(m)} = 0$$

藉由將不同的 $\mathbf{k}_{\parallel}$ 代入上式我們即可得到系統的次能帶結構。

3-1-3. 穿透係數

穿透係數的定義為：

$$T \equiv \frac{J_{transmit}}{J_{incident}} = \frac{\sum_s J_z^{N,s}}{\sum_s J_z^{1,s}}$$

其中 $J_z^{j,s} = \mathrm{Re}[(\varphi^{j,s})^*(-i\frac{\partial}{\partial z}\varphi^{j,s})]$，僅當 $k_z^{j,s}$ 實數的項才會對穿透率有供獻。

3-2 結果與討論

3-2-1. 塊材的複數能帶結構圖
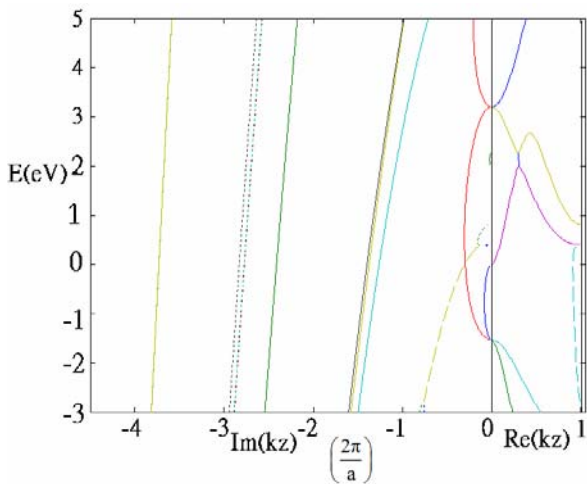
圖 1. 砷化鎵延[001]方向的複數能帶結構圖。
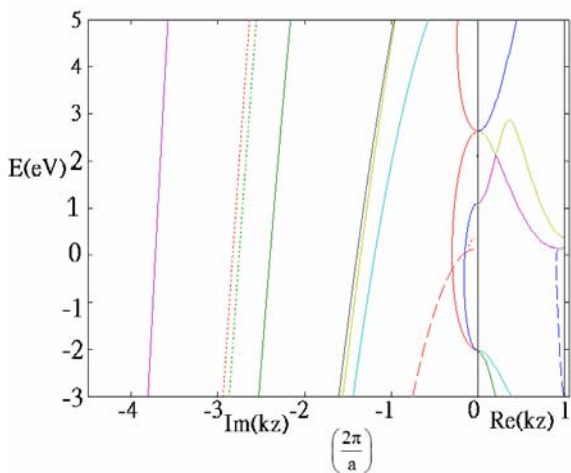
圖 2. 砷化鋁延[001]方向的複數能帶結構圖。

圖一與圖二分別代表砷化鎵與砷化鋁延[001]方向的複數能帶結構圖。在圖中純實數的能帶（$\mathrm{Im}(k_z)=0$）與純虛數的能帶（$\mathrm{Re}(k_z)=0$）用實線來表示且分別置於圖的右側與左側。複數能帶（$\mathrm{Re}(k_z) \neq 0 ; \mathrm{Im}(k_z) \neq 0$）則用虛線或點線來表示，其實部與虛部分別置於圖的右側與左側。點線代表 $\mathrm{Re}(k_z)=2\pi/a$ 的能帶，所以對應點線的實部我們忽略不畫。

由圖一與圖二我們可看出砷化鎵為直接能隙半導體而砷化鋁為間接能隙半導體。我們以砷化鎵導帶的 Γ 點當作是能量的零點，砷化鋁的 Γ 點的能量比砷化鎵高，為 $1.105(\mathrm{eV})$。而砷化鎵的 $\mathbf{X}$ 點的能量為 $0.405(\mathrm{eV})$，相較於砷化鋁的 $0.150(\mathrm{eV})$ 高了 $0.255(\mathrm{eV})$。所以在 Γ 點相對於砷化鎵，砷化鋁是能障；但在 $\mathbf{X}$ 點相對於砷化鋁，砷化鎵是能障。因此若我們適當地將這兩種材料設計成量子井結構，則電子分別會在砷化鎵層與砷化鋁層中形成 $\Gamma-like$ 與 $\mathbf{X}-like$ 的準束縛態(quasi-bound state)因而產生 $\Gamma-\mathbf{X}$ 混成的效應。

3-2-2 次能帶結構與 Γ-$\mathbf{X}$ 混成

由前一節的討論我們知道在砷化鎵/砷化鋁的異質接面結構中會有 $\Gamma-\mathbf{X}$ 混成的現象。因為 $\Gamma-\mathbf{X}$ 混成的現象勢必跟侷限於 Γ 井（也就是砷化鎵層）的 $\Gamma-like$ 波函數與侷限於 X 井（也就是砷化鋁層）的 $\mathbf{X}-like$ 波函數間重疊比例的大小有直接的相關，因此我們預測單位長度中量子井數目越多的結構 $\Gamma-\mathbf{X}$ 混成的效應就會越大。我們將計算結果分成兩部份。第一個部份為實驗組，在固定的長度中增加量子井的數目，我們預期量子井越多 $\Gamma-\mathbf{X}$ 混成越大；第二個部份為對照組，我們固定每一層的厚度下，去增加量子井的數量，觀查 $\Gamma-\mathbf{X}$ 混成的變化。值得一提是，在以下討論中 $\Gamma-\mathbf{X}$ 反交叉能隙（$\Gamma-\mathbf{X}$ anticrossing gap）會是決定 $\Gamma-\mathbf{X}$ 混成效應的重要參數，當反交叉能隙越大代表 $\Gamma-\mathbf{X}$ 混成越嚴重。

3-2-2-1 實驗組:固定總長度下增加量子井數目

以下我們以固定總長度(L)為 130 Å 為例,增加量子井數目觀查其能帶結構圖及穿透率的變化。

(A)一個 *X* 井
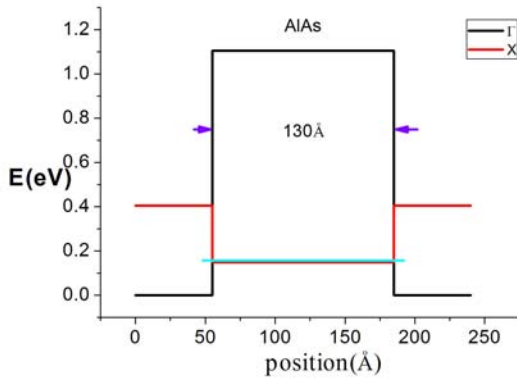
圖 3a. L=130Å,一個 **X** 井時的能帶剖面圖。
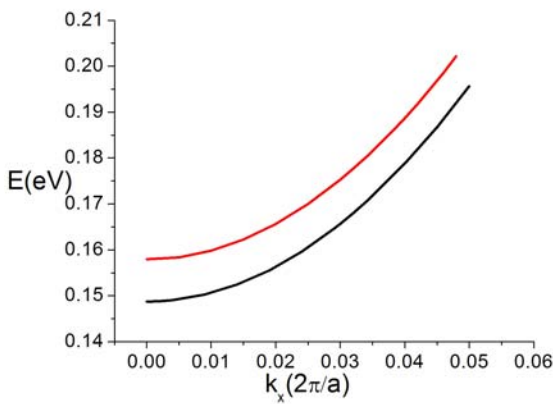
圖 3b. L=130Å,一個 **X** 井時的次能帶結構

在只有一個 **X** 井的情況中(圖 3a),因為沒有由砷化鎵層構成的 Γ 井,所以在此結構中並不會有 Γ−*like* 的準束縛態來造成 Γ−**X** 混成的效應。所以我們看不到其次能帶結構(圖3b)曲率有明顯地變化。

(B)二個 *X* 井
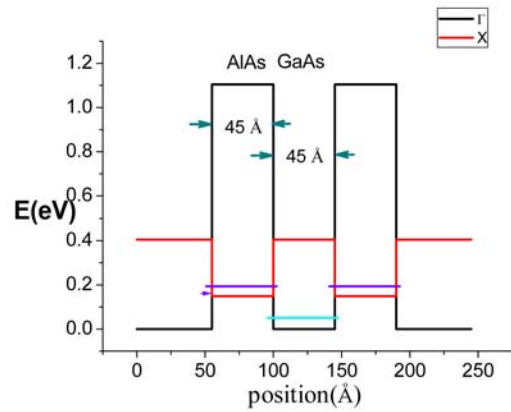
圖 4a. L=130Å,二個 **X** 井時的能帶剖面圖。
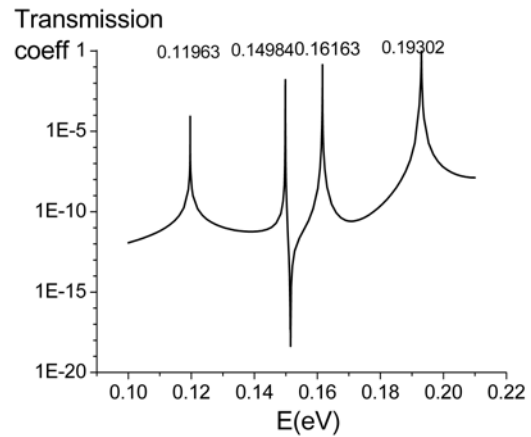
圖 4b. L=130Å,二個 **X** 井時穿透係數對能量的作圖。在此我們考慮入射波在平行量子井方向的波向量($\mathbf{k}_{\parallel}$)為零。
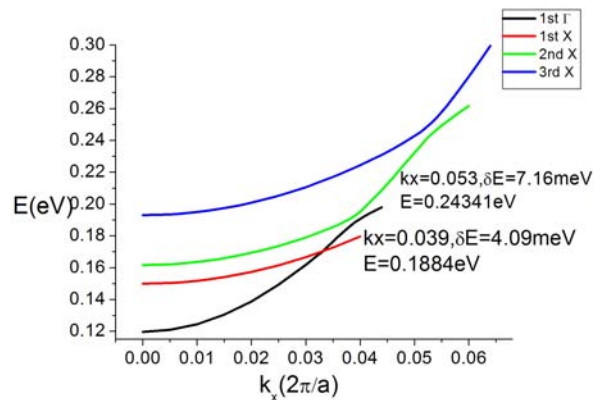
圖 4c. L=130Å,二個 **X** 井時的次能帶結構圖。

相較於（圖 3a）的情況，因為系統包含了二個 X 井（圖 4a），所以此結構多包含了一個 Γ 井（砷化鎵層）來提供 Γ-like 的準束縛態，於是開始有 Γ-X 混成的效應。

（圖 4b）是穿透係數對能量的作圖，我們看到其有四個尖峰。這四個尖峰的能量對應到次能帶結構在 Γ 點（$k_x = 0$）的能量。能量最低的對應到 Γ-like 的準束縛態，而其它三個對應到 X-like 的準束縛態。

由於 Γ-X 混成的效應，相較於（圖 3b）的情況，次能帶結構的曲率開始有明顯的變化（圖 4c）。在（圖 4c）中有兩點值得我們注意。第一，同一條能帶隨著 k_x 的增加每經過一次 Γ-X 混成，能態的特性應會改變一次。原本若為 Γ-like 的態（對應曲率大的能帶）經過 Γ-X 混成會變成 X-like 的態（對應曲率小的能帶），反之亦然。第二，Γ-X 混成若發生在能量較高的能帶，其所對應的 Γ-X 反交叉能隙也會較大。因為一般來說能量越高的能帶所對應的波函數在空間的分佈應會越廣，此時侷限於不同層的 Γ-like（砷化鎵層）與 X-like（砷化鋁層）波函數重疊比例也應越大，所以 Γ-X 混成的效應會越明顯造成較大的反交叉能隙。

(C)三個 X 井
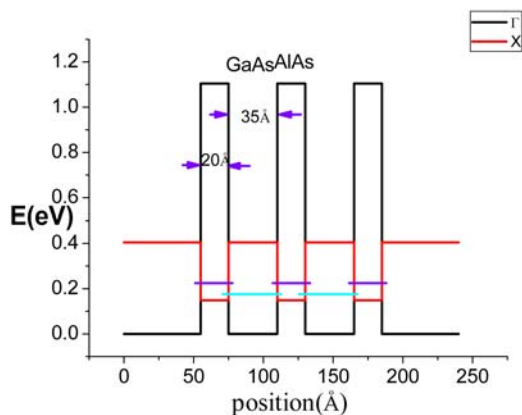
圖 5a. L=130Å，三個 X 井時的能帶剖面圖。
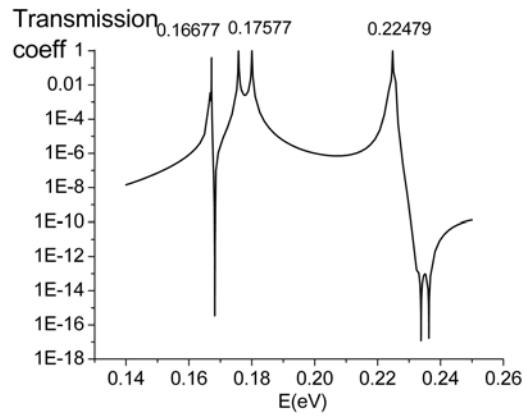
圖 5b. L=130Å，三個 X 井時穿透係數對能量的作圖。在此我們考慮入射波在平行量子井方向的波向量（$\mathbf{k}_\parallel$）為零。
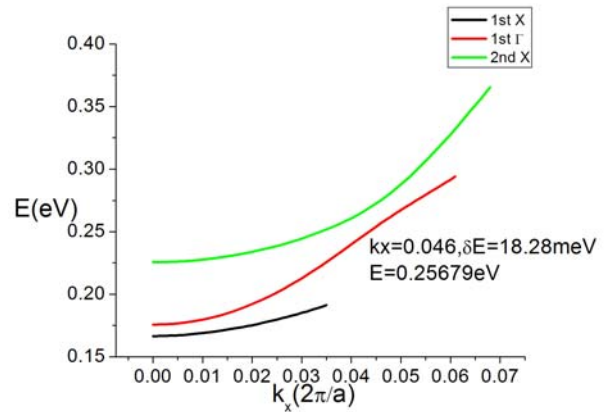
圖 5c. L=130Å，三個 X 井時的次能帶結構圖。

由（圖 5c）我們看到此時第一條與第三條次能帶為 X-like，第二條為 Γ-like。第二條與第三條次能帶會發生第一個 Γ-X 混成。其發生的能量位於 E=0.257(eV)，反交叉能隙的大小為 δE=18.28(meV)。正如我們先前所預測的，與二個 X 井的情況比較（圖 4c），不論是相較於第一反交叉能隙 δE=4.09(meV)，或是與能量相近(E=0.243(eV))的第二反交叉能隙 δE=7.16(meV)比較，三個量子井的情況會有較大的反交叉能隙。

3-2-2-2 對照組:每一層的厚度固定下增加量子井數目

表一 固定總長度為 L=130Å 下增加量子井數目。

	第一反交叉能隙(meV)	第二反交叉能隙(meV)
一個 **X** 井	0	0
二個 **X** 井	4.09	7.16
三個 **X** 井	18.28	

表二 固定總長度為 L=215Å 下增加量子井數目。

	第一反交叉能隙(meV)	第二反交叉能隙(meV)
三個 **X** 井	4.76	7.72
四個 **X** 井	11.86	

表三 固定Γ井厚度 WL=35Å 與 X 井厚度 BL=30Å 下增加量子井數目。

	第一反交叉能隙(meV)
二個 **X** 井	12.56
四個 **X** 井	11.86

表四 固定Γ井厚度 WL=45Å 與 X 井厚度 BL=45Å 下增加量子井數目。

	第一反交叉能隙(meV)	第二反交叉能隙(meV)
二個 **X** 井	4.09	7.16
三個 **X** 井	3.59	7.04

　　為了方便對照起見,我們將實驗組與對照組的計算結果整理列表。表一與表二是實驗組的計算結果,分別代表固定總長度 L=130Å 與 L=215Å 下增加量子井的數目。表三與表四是對照組的計算結果,分別代表固定Γ井厚度 WL=35Å , **X** 井厚度 BL=30Å 與Γ井厚度 WL=45Å , **X** 井厚度 BL=45Å 下增加量子井數目的結果。比較實驗組與對照組我們看到實驗組的反交叉能隙明顯地隨著量子井數目的增加而增加。反之,實驗組的反交叉能隙確似乎與量子井數目沒有明顯地關係。原因是隨著量子井數目的增加實驗組量子井的密度會跟著增加但對照組則否。可以想像隨著量子井數量增加實驗組中侷限於砷化鎵井的Γ態與侷限於

砷化鋁井的 **X** 態波函數重疊的成份應會明顯地增加,但對照組則不會。所以實驗組的反交叉能隙會隨著量子數增而增加,而對照組反交叉能隙的大小則不會與量子井數目有明顯的關係。

四、 文獻

[1] Bradley Ferguson, *Nature Materials* **1**, 26 (2002)

[2] Jian-Bai Xia, *Phys. Rev. B* **41**, 3117 (1990)

[3] Yia-Chung Chang, J. N. Schulman, *Phys. Rev. B* **25**, 3975

[4] David Yuk Kei, J. C. Inkson, *Phys. Rev. B* **37**, 9945 (1988)

[5] A. Zakharova, S. T. Yen, K. A. Chao, *Phys. Rev. B* **64**, 235332 (2001)

Evidence for capture of holes into resonant states in boron-doped silicon

S. T. Yen[a)]
Department of Electronics Engineering, National Chiao Tung University, Hsinchu, 30050 Taiwan

V. N. Tulupenko
Department of Electronics Engineering, National Chiao Tung University, Hsinchu 30050, Taiwan
and Donbass State Mechanical Engineering Academy, Kramatorsk 343913, Ukraine

E. S. Cheng, P. K. Chung, and C. P. Lee
Department of Electronics Engineering, National Chiao Tung University, Hsinchu 30050, Taiwan

A. T. Dalakyan
Department of Electronics Engineering, National Chiao Tung University, Hsinchu 30050 Taiwan
and Donbass State Mechanical Engineering Academy, Kramatorsk 343913, Ukraine

K. A. Chao
Department of Physics, Lund University, Sövegutun 14A, S 233 62 Lund, Sweden

The variation of hole population in the resonant states of B-doped Si excited by sequences of short electric-field pulses has been investigated by the technique of time-resolved step-scan far-infrared spectroscopy. From the variation of the $p_{3/2}$ absorptions, we find that the hole population in the ground state decreases continuously with the sequential electric pulses, as a result of the breakdown delay and hole accumulation in long-lived excited states. The measured time-varying spectra of the $p_{1/2}$ series have been analyzed and attributed to a significant variation of the hole population in the resonant states. We have also observed a new absorption line at 676 cm^{-1} which is probably caused by the electric-field induced mixing of the resonant states. © *2004 American Institute of Physics.*
[DOI: 10.1063/1.1795985]

I. INTRODUCTION

The electronic states of an impurity in semiconductors are regarded as resonant states when they are degenerate in energy with one or more continua of the band structure, a notion originating from Fano.[1] One of the most common types of resonant states is the classical one of acceptor states that are associated with the spin-orbit $p_{1/2}$ bands and degenerate with the continua of the $p_{3/2}$ bands in cubic semiconductors. The existence of such resonant acceptor states was first verified by Zwerdling *et al.* more than four decades ago by observation of the $p_{1/2}$ excitation spectrum from B- and Al-doped Si.[2] With the advance in techniques of sample preparation and infrared spectroscopy the excitation spectra have been resolved more accurately and reassigned for the $p_{1/2}$ resonant states as well as the $p_{3/2}$ localized states of various Group III acceptors (B, Al, Ga, and In) in Si.[3–6] Theoretical formulations for the resonant states have been developed and so far the calculated results can supply a quantitative interpretation for the measured absorption lines.[7,8]

Although the problem of resonant states in semiconductors seems not new, the possibility of terahertz (THz) emission in doped semiconductors has renewed interests of researchers to it in the last decade since the THz radiation can be connected with the electric-dipole transition from one of the resonant states to a localized state.[9,10] The stimulated emission and lasing operation of THz waves have been real-ized from *p* type uniaxially deformed Ge with the electric field and the external stress being in parallel[10–12] and also in crossing[13] configurations. The THz gain has been attributed to the population inversion of holes between the resonant states attached to the heavy-hole bands and the localized states attached to the light-hole bands, where the capture of holes from continuous band states into the resonant states plays a key part.[9,14] Based on an analogous mechanism, possibilities of THz radiation from *p*-doped strained SiGe (Ref. 15) and quantum wells with resonant impurity states[16] have been proposed without the external applied stress. So far, however, there has not yet been any direct experimental evidence for the hole capture by the resonant states.

In this paper, we report an experimental evidence for capture of holes into the $p_{1/2}$ resonant states in B-doped silicon under sufficiently high electric-field pulses. The main idea of the experiment is to observe the time-varying absorptions of both the $p_{1/2}$ and $p_{3/2}$ series for B-doped Si excited by sequences of electric pulses, using the technique of time-resolved (TR) step-scan spectroscopy. This observation can reveal information on the evolution of hole populations in the various types of acceptor states. The reasons for using B-doped Si are as follows. The binding energy of the ground state of B ($\varepsilon_B = 45$ meV) is the smallest among those of the Group III acceptors in Si, rendering the holes in B-doped Si more likely to be ionized in a moderate electric field at a low temperature. Secondly, the oscillator strength of transitions associated with the $p_{1/2}$ lines is the largest for B compared with other Group III species in Si.[8] Furthermore, the optical phonon energy ($\varepsilon_{op} = 63$ meV) for Si is larger than the spin-

a)Electronic mail: styen@faculty.nctu.edu.tw

4970
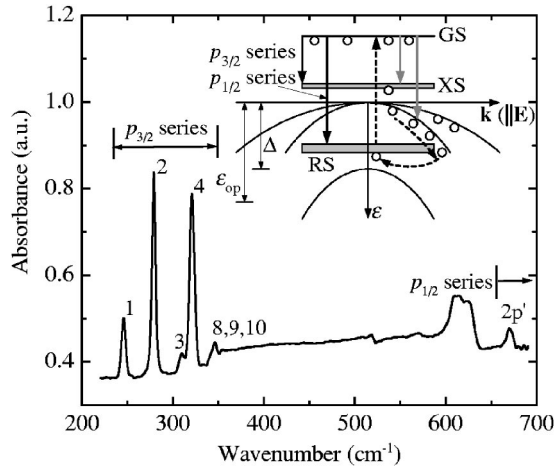
FIG. 1. The absorption spectrum for boron in silicon taken in the absence of external fields at 20 K. The inset illustrates the hole excitation and acceleration by the electric field, the hole capture into the resonant states, and the transitions for the $p_{1/2}$ and $p_{3/2}$ absorptions, where the abbreviations GS, XR, and RS stand for the ground states, the localized excited states, and the resonant states, respectively, of acceptors.

orbit split-off energy ($\Delta = 44$ meV) between the $p_{1/2}$ and the $p_{3/2}$ bands. It follows that with a low impurity concentration and at a low temperature, there is a high probability for the ionized holes to gain sufficient kinetic energy ε in a high electric field to reach the energy of the resonant states before emitting an optical phonon, as illustrated in the inset of Fig. 1. In this situation the hole distribution in the momentum space will strongly displace from an isotropic one as a consequence of cyclic streaming motion in which optical phonon scattering is predominant.[17] The average energy of the holes would be high enough and a considerable amount of holes can have kinetic energy in the range $\varepsilon_B < \varepsilon < \varepsilon_{op}$ so that they can play parts in the impact ionization of holes from the localized states. It is therefore possible for holes in B-doped Si under an appropriate electric field to achieve an ideal distribution for population inversion in such a way that the distribution function be narrow with its maximum at the energy of the resonant state while the localized states remain depopulated.[9,14] Naturally, one would expect accumulation of holes in the resonant states through resonance scattering or other paths. Such a picture is difficult to achieve for Si doped with other species of acceptors that have a higher binding energy of holes. It is also hardly possible for p-type Ge that has a large spin-off energy Δ because the optical phonon scattering will prevent carriers from gaining enough kinetic energy to reach the energy of the resonant state. For polar semiconductors, strong accoustic phonon interaction would cause the distribution of carriers to be broadening in the momentum space, making them also unfit for the population inversion.

II. EXPERIMENT

The experiment was performed using samples with dimensions of 6×12 mm^2 cut along the [001] crystallographic axes from a 0.5 mm thick (100) B-doped Czochralski Si wafer of a room-temperature resistivity of 8Ω cm. The acceptor concentration in the samples is estimated to be about 1.5

$\times 10^{15}$ cm^{-3}.[18] Two contacts with area of 6×4 mm^2 were made using Al on one surface of the samples, leaving a central 6×4 mm^2 window for spectroscopic measurement. One of the samples was then treated for Ohmic contacts with annealing at $350\,°$C for 30 min. The I-V curves measured from the sample in a pulse mode ensure that the contacts are Ohmic up to 1000 V. Each of the metallic contacts was then soldered together with a piece of $1 \times 18 \times 6$ mm^3 copper using pure indium to improve the cooling efficiency of the sample in exchange gas of the continuous flow cryostat. Special design and tools were used to keep the indium thickness of being 0.45 mm. One of the copper holders was fixed to the finger of the cryostat while the other was left free. Such a scheme of making contacts and fixing the sample was used to alleviate the Joule heating and possible mechanical strain in Si. Rapid-scan spectra with resolution of 2.5 cm^{-1} were taken from the sample in the aforementioned scheme and from another one mounted to the cryostat finger with a thin teflon film. No difference was found between the spectra in the absence of electric fields.

The cryostat with the sample was put into an IFS66v/S Fourier transform infrared (FTIR) spectrometer in such a way that the sample was capable of being irradiated by light from the FTIR source through the window between the contacts. In front of the sample was put symmetrically a screen with a 5×2.5 mm^2 hole, made of stainless foil covered by black paper to prevent the light from passing through the boundary sides into the sample. A He-cooled Si bolometer was used as a detector. Equipped with a polyethylene filter, a Mylar-3.5 μm beam splitter, and KRS5 windows for the cryostat, the spectrometer allows one to measure spectra of interest in the range from 240 to 685 cm^{-1}.

To avoid overheating of the sample the electric field was applied in the burst mode. There were 50 pulses in a burst. The pulse duration was 0.2 μs and the duty cycle was 0.01. The duration of each burst is thus 1 ms. The repetition rate of the bursts was 15.6 Hz. The Joule heating by the pulses led to a moderate increase in the environmental temperature from a temperature T_0 (measured in the absence of electric fields) to a higher temperature T^*. These temperatures were registered by a Ge thermoresistor with a time constant of 100 ms mounted on one of the copper pieces.

To increase the signal-to-noise ratio, 100 sets of data were recorded and coadded for each interferogram using the TR step-scan technique. There were 884 points in the interferogram demanded for an optical resolution of 2.5 cm^{-1} and a phase resolution of 15 cm^{-1}. These parameters were a consequence of compromise between the resolution for distinguishing the absorption lines of interest and the time consumption for the measurement. Just before starting a real ac coupled TR measurement, we took a quick dc coupled TR interferogram in the absence of electric fields for further phase correction of the measured AC spectra. The obtained single-channel TR spectra $\Delta S(\nu, t)$ were further processed to get the corresponding delta absorbance spectra ΔA according to the formula

TABLE I. Some of parameters for three sets A, B, and C of spectra: the temperature (T_0) in the absence of electric fields, the average temperature (T^*), the applied voltage (V), the electric field (E), and the time resolution $(\Delta\tau)$. The other parameters such as the pulse width (0.2 μs), the duty circle (0.01), and the number of pulses in a burst (50) are the same for the three sets of spectra.

Spectra	T_0 (K)	T^*(K)	V (V)	E(V/cm)	$\Delta\tau$ (μs)
A	20	27	740	1850	40
B	24	27	530	1300	40
C	45	53	500	1250	20

$$\Delta A(\nu,t) = -\ln\left[1 + \frac{\Delta S(\nu,t)}{S_0(\nu)}\right], \tag{1}$$

where $S_0(\nu)$, serving as a reference, is the ac coupled rapid-scan single-channel spectrum measured at T^* but in the absence of electric fields.

III. RESULTS AND DISCUSSION

The absorption line $2p'$ and lines 1, 2, 3, and 4 (in notation of Onton *et al.*[3]) which are of main interest in the present work can be well resolved. Figure 1 shows the spectra measured at 20 K in the absence of electric fields. The positions of the lines are in agreement with the data of Onton *et al.*[3]

We took three sets, A, B, and C, of electroabsorption spectra in the experiment. In Table I Iare listed some of the parameters adopted for measuring the three sets of spectra, such as the temperatures T_0 and T^*, the applied voltage V, the electric field E, and the time resolution $\Delta\tau$. The other parameters which are not listed, such as the pulse width (0.2 μs), the duty cycle (0.01), and the number of pulses (50) in a burst, are the same for the three sets of spectra. The period of time slices at which the data were taken is set to equal the time resolution $\Delta\tau$. We took $\Delta\tau$=40 μs for spectra A and B, and 20 μs for spectra C. It should be pointed out that in spite of the very short time duration $\Delta\tau$ compared with the time constant ($\sim$1 ms) of the bolometer, the high sensitivity of the bolometer and the wide dynamic range of a 16-bit analog-to-digital converter in FTIR allow us to observe the variation of optical signals with the time slices. The resulting electroabsorption spectra are shown in Fig. 2, where we show from the two sets A and B the spectra recorded at the first 11 time slices (slices 0–10) but from the set C the spectra at the first 11 each-third time slices (slices $0, 3, 6, \ldots, 30$). Here, each of the first time slices, labeled with 0, was synchronized with the beginning of the bursts. We can see from the spectra that the values of delta absorbance ΔA of $p_{3/2}$ lines 1 (at 245 cm^{-1}), 2 (at 278 cm^{-1}), and 4 (at 319 cm^{-1}) are positive at the first several slices (slices 0–3 for spectra A and B and slices 0–9 for spectra C). This means that the absorptions measured at the first several time slices are larger than the reference absorption measured at T^* in the absence of electric fields. The larger absorption may be attributed to a higher concentration N_G of holes in the ground state or a lower concentration N_{LX} of holes in the localized excited states since the absorption is proportional to the difference $N_G - N_{LX}$ for the optical transition from the ground state to
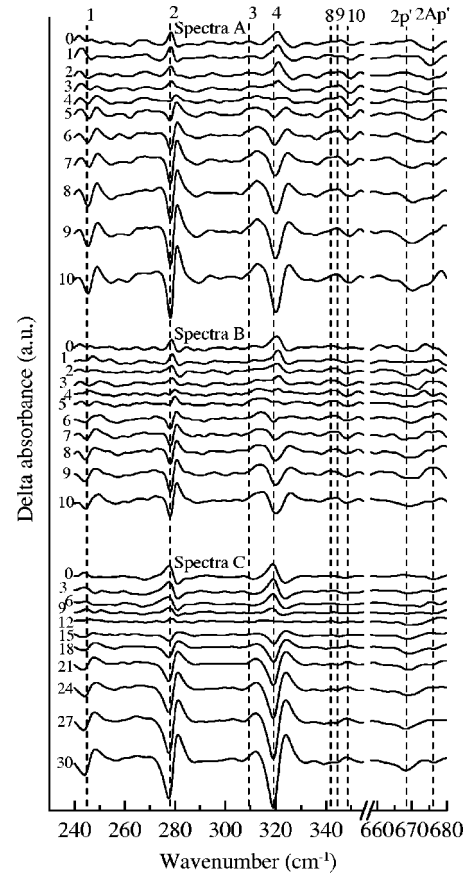
FIG. 2. The three sets, A, B, and C, of electroabsorption spectra taken at different time slices for boron in silicon excited by sequential electric-field pulses. The parameters for the three sets of spectra are listed in Table I.

the localized excited states. As will be demonstrated later, the lattice temperature T_L is dropping during the initial time slices as well as before the beginning of the bursts. This temperature dropping increases N_G while reduces N_{LX} before the first electric pulse is applied. The successive electric pulses can then remove holes from the localized acceptor states to shallower ones or to the continuous band states. Holes bound to shallower states are more likely ionized through either the Zener tunneling or the impact process when the electric field is applied. Only a smaller fraction of holes from the deeper ground state are excited by each of the short pulses of electric fields (E=1850, 1300, and 1250 V/cm for spectra A, B, and C, respectively) due to the large separation in energy from the excited states.[19] As a consequence, at the initial time slices when the free hole concentration p is small and thus the hole capture from the continuous band states is neglected, more holes are removed from a shallower acceptor state than from a deeper one by the electric pulses. The argument described above can also be supported by the difference in the magnitude of the delta absorbance of lines 1, 2, and 4 at the first time slices, where $\Delta A_4 > \Delta A_2 > \Delta A_1$ (ΔA_i being the delta absorbance of line i).

It is also a common feature of the spectra that the $p_{3/2}$ absorptions of lines 1, 2, and 4 decrease monotonically with the time slices. While this may be due to the increase in the lattice temperature T_L caused by the Joule heating of the sequential electric pulses, a further investigation of the tem-
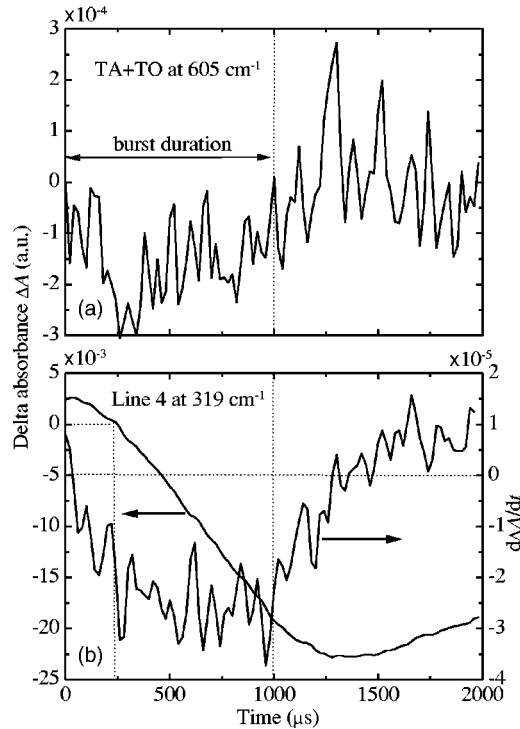
FIG. 3. The delta absorbance (a) for the multiphonon (TA+TO) process at 605 cm^{-1} and (b) for line 4 at 319 cm^{-1} as functions of time. Also shown in panel (b) is the derivative of the delta absorbance for line 4 with respect to time. The data were taken from spectra C at T_0=45 K, T^*=53 K, and E =1250 V/cm.

perature variation with time slices rules out the simple interpretation. In fact, T_L drops rather than rises during the first time slices, since there are a small amount of free holes available to generate Joule heating. This is also evident from Fig. 3(a) where the temporal variation of the delta absorbance at 605 cm^{-1} was recorded from spectra C. The absorption at 605 cm^{-1} has been known as the lattice absorption of bulk Si associated with the process of absorption of a photon and emission of two phonons (TA+TO).[20] Such a multiphonon absorption increases with T_L rising. With the aid of the temperature dependence of the absorption at 605 cm^{-1}, we can read from Fig. 3(a), in spite of the small signal-to-noise ratio, that the lattice temperature for spectra C still dropped during the initial 300 μs (corresponding to the first 15 time slices) but then rised until the temporal point approximately at 1250 μs which is 250 μs after the end of the bursts. The lag of the T_L variation to the switching of electric-field heating is obviously caused by the lower heat generation rate compared with the rate of heat drained by the cryostat. We expect similar temperature variations for spectra A and B although a significant variation of the absorption at 605 cm^{-1} was not observed due to the low temperature (T_0/T^*=20 K/27 K and 24 K/27 K for spectra A and B, respectively).[20] On the basis of the preceding argument, we suggest that the variation of the $p_{3/2}$ absorptions are not simply dominated by the temperature variation. The decrease in the $p_{3/2}$ absorptions must result mainly from continuous depopulation of the holes in the ground state by the sequential electric-field pulses, accompanied with accumulation of holes in the excited states in the duration between two near-

est pulses. After an electric-field pulse passing, a majority of the excess free holes in the absence of electric fields are captured from continuous band states to localized excited impurity states in a short time and then would cascade to the ground state if the next electric pulse came a sufficiently long time later.[21] However, the duration between two nearest pulses (20 μs) appears not long enough for the holes to complete a transition from the excited to the ground states; otherwise, the system would return to a thermal-equilibrium state before the next pulse came and, in this case, the absorption strength would simply be a function of temperature only. We conclude that there must exist long-lived (LL) excited states in B-doped silicon so that the hole accumulation in these states occurs in the duration between two nearest pulses. The existence of such long-lived states has also been experimentally confirmed by Lehto and Proctor[19] and more recently by Pokrovskiĭ *et al.*[22] A small fraction of holes in the ground state as well as a majority of the holes in the excited states (including the LL states and other excited states) are then released to the band by the application of the next electric pulse. As a consequence, the ground state population N_G drops continuously with the time slices while the concentration p of free holes increases. (The values are average over the time resolution $\Delta\tau$.) Because of the high capture rate of holes from the continuous band states to the excited states, the excited state population N_{LX} is expected to be strongly related with p; that is, N_{LX} also increases continuously with the time slices. The depopulation of the ground state is more enhanced for a higher electric field and also at a higher temperature, as can be seen from the three sets of absorption spectra A, B, and C. This is because a higher electric field can reduce the breakdown delay and excite more holes from the ground state in the short pulse duration.[19] The efficiency of the impact excitation depends also upon the concentration of initial free holes in the continuous band states.[19] At a higher temperature or at a latter time slice where there are more initial free holes, the population N_G decreases and N_{LX} increases more rapidly. This explains the more noticeable decrease in delta absorbance of lines 1, 2, and 4 at latter time slices and at a higher temperature (for spectra C). With the picture described, it is not difficult to understand the variations of ΔA_4 and $d\Delta A_4/dt$ with time, as shown in Fig. 3(b). The absorption ΔA_4 first slightly increases (with positive $d\Delta A_4/dt$) because the effect of T_L dropping dominates over that of the accummulation of LL holes which then becomes dominant. The heating is more and more important with the time since more and more free holes are available for generating heat. At 250 μs when the heat generated is balanced with that drained out, T_L reaches the minimum, as can be seen from Fig. 3(a). After this time, T_L then becomes increasing, enhancing the decrease of ΔA_4 as can be seen from Fig. 3(b). A very recent observation of THz electroluminescence from B-doped Si can also serve as an additional evidence for the existence of the long-lived excited states and the depopulation of the ground state with successive electric pulses.[23]

　　Now let us turn our attention to the $p_{1/2}$ lines in Fig. 2 (see also Fig. 4 for clarity), which are associated with the electric-dipole transitions from the ground state to the reso-
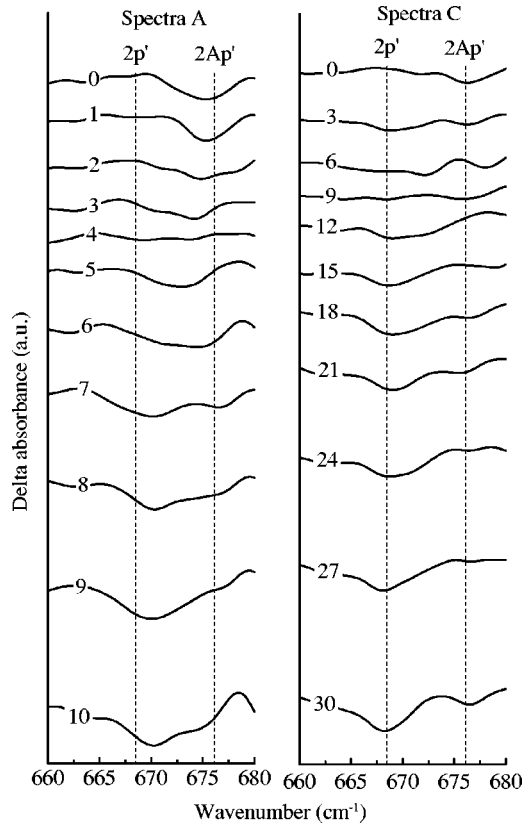
FIG. 4. The electroabsorption spectra in the range of large wave number. The left panel is taken from spectra *A* and the right panel is taken from spectra *C* in Fig. 2.

nant states. The $2p'$ line at 668 cm^{-1} and the $3p'$ line at 693 cm^{-1} have been observed for B-doped Si in the absence of electric fields,[2,3,5] while the line marked $2Ap'$ at 676 cm^{-1} has never been reported. According to the calculated results of Buczko and Bassani,[8] there are two energy levels close in energy to the first resonant state Γ_6^-; one is the fourfold degenerate level Γ_8^- located at 0.08 meV (in electronic energy) below Γ_6^- and the other is a twofold degenerate level Γ_7^+ at 0.95 meV below Γ_6^-. The line $2Ap'$ has the wave number associated with the transition from the ground states (Γ_8^+) to the Γ_7^+ states, which is nearly forbidden in the absence of electric fields due to the same parity of the envelope functions of the Γ_8^+ and Γ_7^+ states. (Note that the total wave functions lack a definite parity since the system lacks the inversion symmetry.) However, under an electric field applied along the [001] direction, the symmetry of the system reduces from the T_d group to the D_{2d} group. Consequently, the three energy levels of the resonant states $\Gamma_6^- + \Gamma_7^+ + \Gamma_8^-$ are hybridized together and split into four energy levels $2\Gamma_6 + 2\Gamma_7$ (Γ_6 and Γ_7 being the irreducible representations of D_{2d}) in a sufficiently strong electric field. Based on the estimation $\langle r \rangle eE > 1.5$ meV, where $\langle r \rangle > 150$ Å is the mean radius of the resonant states[8] and e the electronic charge, we expect a considerable mixing of the resonant states by the external fields. In this situation, the selection rule is no longer valid and the variation of the $2Ap'$ absorption becomes observable, as Fig. 2 shows. In contrast to the $p_{3/2}$ absorptions, the $p_{1/2}$ absorptions are smaller at almost all the time slices than the reference absorption measured in the absence of electric

fields because of the nonpositive delta absorbance of the $p_{1/2}$ lines. This means that the T_L dropping and the electric fields at the initial time slices do not cause a decrease in the hole population of the resonant states. Instead, the population in the resonant states increases since the negative delta absorbance of the $2Ap'$ line cannot be explained simply by the decrease in the ground state population N_G. As has been described previously, N_G decreases during the first time slice because of the application of the electric pulses. It is an important finding that the negative delta absorbance moves from $2Ap'$ to $2p'$ with the time slices. We attribute the phenomenon to a transfer of the excess captured holes from the high-energy resonant state to the low-energy one or probably to the $p_{3/2}$ band states through resonant escape. The negative delta absorbance of the $2p'$ line at latter time slices can be explained by the decrease in the ground state population or the increase in the population of the first resonant state. Such relaxation processes involving the resonant states appear complicated and require further experimental and theoretical investigations for identification.

IV. CONCLUSION

In conclusion, we have observed the variations of the hole populations in the ground, resonant, and localized excited states for B-doped Si under trains of electric-field pulses by the technique of TR far-infrared electroabsorption spectroscopy. The ground state population decreases monotonically with the successive short electric pulses because of the breakdown delay and the hole accumulation in the long-lived excited states. We have also observed the $2Ap'$ absorption line at 676 cm^{-1} which is believed to be caused by the electric-field induced mixing of the resonant states. The population of excess holes in the high-energy resonant state has been observed. As time goes on, the holes may transfer to the low-energy state or escape to the continuous band states.

ACKNOWLEDGMENTS

[1]See, e.g., F. Bassani, G. Iadonisi, and B. Preziosi, Rep. Prog. Phys. **37**, 1099 (1974).
[2]S. Zwerdling, K. J. Button, B. Lax, and L. M. Roth, Phys. Rev. Lett. **4**, 173 (1960).
[3]A. Onton, P. Fisher, and A. K. Ramdas, Phys. Rev. **163**, 686 (1967).
[4]J. J. Rome, R. J. Spry, T. C. Chandler, G. J. Brown, B. C. Covington, and R. J. Harris, Phys. Rev. B **25**, 3615 (1982).
[5]D. W. Fischer and J. J. Rome, Phys. Rev. B **27**, 4826 (1983).
[6]For a review of experimental results obtained up till 1981 on the spectroscopy of acceptors in semiconductors together with the theory for their interpretation, see A. K. Ramdas and S. Rodriguez, Rep. Prog. Phys. **44**, 1297 (1981).
[7]F. Bassani, G. Iadonisi, and B. Preziosi, Phys. Rev. **186**, 735 (1969).
[8]R. Buczko and F. Bassani, Phys. Rev. B **45**, 5838 (1992).
[9]M. A. Odnoblyudov, I. N. Yassievich, M. S. Kagan, Y. M. Galperin, and K. A. Chao, Phys. Rev. Lett. **83**, 644 (1999).
[10]I. V. Altukhov, M. S. Kagan, K. A. Korolev, V. P. Sinis, E. G. Chirkova, M. A. Odnoblyudov, and I. N. Yassievich, JETP **88**, 51 (1999).

J. Appl. Phys., Vol. 96, No. 9, 1 November 2004

Yen *et al.* 4975

[11]I. V. Altukhov, M. S. Kagan, K. A. Korolev, V. P. Sinis, and F. A. Smirnov, Sov. Phys. JETP **74**, 404 (1992).

[12]Y. P. Gousev, *et al.*, Appl. Phys. Lett. **75**, 757 (1999).

[13]V. N. Bondar, A. T. Dalakyan, L. E. Vorob'ev, D. A. Firsov, and V. N. Tulupenko, JETP Lett. **70**, 265 (1999).

[14]M. A. Odnoblyudov, I. N. Yassievich, V. M. Chistyakov, and K. A. Chao, Phys. Rev. B **62**, 2486 (2000).

[15]A. Blom, M. A. Odnoblyudov, H. H. Cheng, I. N. Yassievich, and K. A. Chao, Appl. Phys. Lett. **79**, 713 (2001).

[16]S. T. Yen, Phys. Rev. B **66**, 075340 (2002).

[17]W. E. Pinson and R. Bray, Phys. Rev. **136**, A1449 (1964).

[18]S. M. Sze, *Physics of Semiconductor Devices*, 2nd ed. (Wiley, New York, 1981), p. 32.

[19]A. Lehto and W. G. Proctor, J. Phys. C **11**, 2239 (1978).

[20]F. A. Johnson, Proc. Phys. Soc. London **73**, 265 (1959).

[21]M. Lax, Phys. Rev. **119**, 1502 (1960).

[22]Ya. E. Pokrovskiǐ, O. I. Smirnova, and N. A. Khvalkovskiǐ, JETP **85**, 121 (1997); **90**, 404 (2000).

[23]T. N. Adam, R. T. Troegger, S. K. Ray, P.-C. Lv, and J. Kolodzey, Appl. Phys. Lett. **83**, 1713 (2003).